Mode-locking Instabilities for High-Gain Semiconductor Disk Lasers Based on Active Submonolayer Quantum Dots

C. G. E. Alfieri,[1,*] D. Waldburger,[1] J. Nürnberg,[1] M. Golling,[1] L. Jaurigue,[2] K. Lüdge,[2] and U. Keller[1]

[1]*Department of Physics, Institute for Quantum Electronics, ETH Zurich, Switzerland*
[2]*Institut für Theoretische Physik, TU Berlin, Berlin, Germany*

Submonolayer quantum dots (SML QDs) combine the large gain cross section of quantum wells (QWs) with the potential benefits of a stronger confinement. We demonstrate here an optically pumped vertical external-cavity surface emitting laser (VECSEL) based on active SML QDs. The ultrafast SML QD VECSEL is optimized for passive modelocking with an intracavity semiconductor saturable absorber mirror (SESAM) around 1030 nm. We have achieved the highest cw output power of 11.2 W from a QD-based VECSEL to date. With a birefringent filter inside the VECSEL cavity, we obtain a tuning range of 47 nm centered at 1028 nm. Any attempt to passively modelock the VECSEL with a QW SESAM reveals fundamental limitations. The intrinsically higher linewidth enhancement factor of SML QDs compared to QWs or self-assembled Stranski-Krastanov QDs is further increased at higher pump powers. Our experiments confirm prior theoretical predictions that a strong amplitude-phase coupling can destabilize cw modelocking and introduce chaotic multiple pulse fluctuations.

I. INTRODUCTION

Optically pumped passively modelocked vertical external-cavity surface-emitting lasers (VECSELs) [1–3] and modelocked integrated external-cavity surface-emitting lasers (MIXSELs) [4] are also referred to as ultrafast semiconductor disk lasers (SDLs). SDLs represent a compact and wavelength-flexible solution for diverse application fields such as dual-comb spectroscopy [5] and multiphoton imaging [6]. The best SDLs in terms of output power perform in the 1-μm spectral region, where they can benefit from the high-index contrast, lattice-matched GaAs/AlAs material systems. Thanks to the high modal gain provided by active $(In_xGa_{1-x})As$ quantum wells (QWs), output powers up to 106 W could be demonstrated in cw operation [7]. Passive modelocking was achieved with semiconductor saturable absorber mirrors (SESAMs) [8] with the first demonstration in 2000 [9]. Since then, record ultrafast results have been demonstrated with an optically pumped MIXSEL generating picosecond pulses and more than 6 W of average power [10], with a quantum dot (QD) VECSEL generating femtosecond pulses with more than 1 W average power [11], with a MIXSEL with scalable pulse repetition rates between 5 and 100 GHz [12], and with record low noise performance very similar to diode-pumped solid-state lasers [13]. The simple straight cavity of a MIXSEL inspired the invention of

dual-comb modelocking [14] and the successful proof-of-principle demonstration of dual-comb molecular spectroscopy using only one unstabilized semiconductor laser (i.e., dual-comb MIXSEL) [5], which can be considered a paradigm shift in frequency metrology applications.

One of our research efforts is focused on the optimization of ultrafast SDLs toward femtosecond high-power operation with sufficient pulse peak power to generate a coherent supercontinuum without the external pulse amplification demonstrated before [15,16]. With SESAM-modelocked QW VECSELs, we obtained pulses as short as 100 fs [17] and with QW MIXSELs as short as 184 fs [18] with an average output power around 100 mW. However, ultrafast QW SDLs suffer from spectral hole-burning effects [18,19], which currently seem to limit further pulse shortening with high-pulse energy. Furthermore, the high nonradiative losses reduce the carrier lifetime in the active QWs, drastically decreasing the optical-to-optical efficiency of sub-300-fs SDLs to below 1% [18]. Ultrafast SDLs based on self-assembled QDs grown by the Stranski-Krastanov (SK) method can benefit from some key advantages over QWs due to their broadband emission, temperature insensitivity, and fast gain recovery [20–22]. To date, SK QD VECSELs have demonstrated broadband tunability up to 69 nm in cw operation [23] and recently achieved pulses as short as 193 fs with relatively high optical-to-optical efficiency [24]. The trade-off is that the QD areal density achievable with the SK epitaxial technique is typically limited to 10^{10}–10^{11} cm^{-2} [25,26], which

---

results in a reduced density of states (DOS) and therefore lower available optical gain. For this reason, the highest output power reported for a QD VECSEL is limited to 8.4 W in cw operation [27].

In this paper, we want to explore the potential of submonolayer (SML) QDs [28] as active media for high-peak-power ultrafast SDLs. The growth of SML superlattices involves a cycled deposition of InAs submonolayers capped with a few monolayers of GaAs, creating a vertically correlated InAs agglomeration with typically high areal densities of the order of 10^{12} cm^{-2} [29]. The heterodimensional morphology of SML QDs combines the beneficial signatures of a zero-dimensional (0D) confinement such as high excitonic gain and very fast gain dynamics with the large DOS and high modal gain usually featured by 2D-confined structures [30]. In addition, the absence of a wetting layer prevents detrimental carrier trapping in states not contributing to lasing and makes SML QDs particularly suited for high-speed optoelectronic devices [31,32]. To date, SML VECSELs have been tested only in cw operation, where the maximum reported output power of 1.4 W was obtained at 1034 nm [33]. No modelocking has ever been tried with such devices.

Here, we report on a high-power SML QD VECSEL. Even if the semiconductor epitaxial layer stack is designed and optimized for ultrafast operation and not for high-power cw operation, we can demonstrate up to 11.2 W cw output power at 1028 nm - the highest output power from any QD VECSEL to date. We characterize the wavelength tunability of the device and obtain lasing operation from 1003 to 1050 nm, with high output powers above 1 W from 1008 to 1044 nm, confirming the large gain bandwidth of the structure and the high modal gain delivered by SML QDs.

However, despite the promising cw lasing performance, we show here that any attempts to SESAM-modelock the SML QD VECSEL do not produce the expected better ultrafast performance. A limited-stability mode-locking result is obtained only for short periods (<5 min) just above the lasing threshold, with pulses not shorter than 1.18 ps at a repetition rate of 1.65 GHz and an average output power of 84 mW. At higher pump levels, the laser becomes unstable with intermittent transitions from cw modelocking to irregular spikings and multi-pulse fluctuations. This noisy behavior can be explained by the strong amplitude-phase coupling in SML QDs typically characterized by the linewidth enhancement factor (α factor) [34, 35]. With this result, we present experimental verification of theoretical predictions by models of passive modelocking in semiconductor lasers from more than 10 years ago [36]. We can also justify these theoretical predictions with our pulse formation model [37] which confirms a sudden breakup of stable cw modelocking to a chaotic behavior with increasing gain linewidth enhancement factors. This

leads us to the conclusion that SML QDs are not suited for ultrafast SDLs.

II. VECSEL DESIGN, GROWTH, AND CHARACTERIZATION

The SML QD VECSEL described in this work is grown using molecular beam epitaxy (MBE) on undoped 100-oriented GaAs substrates. The VECSEL gain is optimized for lasing operation at 1030 nm. The VECSEL chip epitaxial stack [Fig. 1(a)] shows, starting from the bottom, the last few layers of a 23.5-pair AlAs-GaAs distributed Bragg reflector (DBR), followed by an active region featuring 10 SML QD layers embedded in pump-absorbing GaAs barriers, and finally an antireflection (AR) coating section. Each SML QD layer is formed by a tenfold alternate deposition of pure binary InAs and GaAs. The short superlattice period consists nominally of 0.4 monolayers (ML) InAs and 2.1 ML GaAs. A single InAs deposition stays below the critical thickness required by SK QD formation and creates islands, which are immediately buried by the GaAs spacer. The larger lattice constant of InAs compared to GaAs produces local tensile strain in the GaAs coverage where it occurs to cap an InAs island. The locally increased
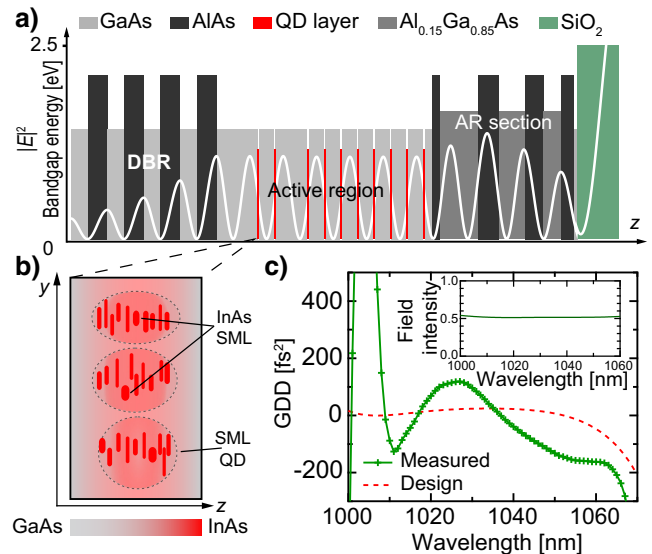

FIG. 1.   SML QD VECSEL. (a) Schematic of the SML VECSEL's epitaxial structure: bandgap profile and calculated electric-field intensity (white). Note that only the last few layers of the bottom 23.5-pair AlAs-GaAs distributed Bragg reflector (DBR) are shown. (b) A schematic view of a single SML-QD layer with a ten-fold InAs SML deposition (red dashes). Indium diffusion creates a vertical correlation between the SML islands and forms the SML QD (dashed ovals). (c) Measured and designed dispersion of the VECSEL gain mirror. The measurement is performed at normal incidence and room temperature. Inset: designed average field intensity in the QD layers, optimized to be flat over a broad wavelength bandwidth around the lasing center wavelength to avoid structural spectral filtering.
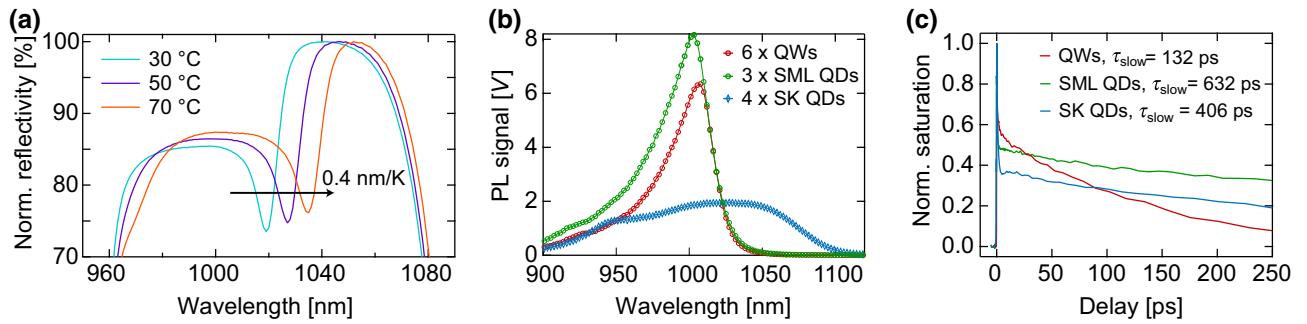
FIG. 2. SML QD VECSEL characterization. (a) Reflectivity measurements of the unpumped SML QD VECSEL at different temperatures. The absorption of the SML QDs presents a temperature-dependent redshift of 0.4 nm/K, similar to that observed for QWs. (b) PL measurements of different active test structures based on SML QDs, QWs, and SK QDs. Three SML QD layers without strain compensation show a higher PL intensity than 6 QW layers with strain compensation and comparable FWHM emission bandwidth (40 and 37 nm, respectively). SK QDs feature the lowest intensity, but also the broadest bandwidth of 134 nm. (c) Degenerate pump-probe measurement of a SMLs', QWs', and SK VECSELs' saturation. The pump fluence is set to 30 μJ/cm^2. QDs show a long carrier lifetime compared to QWs.

lattice constant facilitates the successive nucleation of the following InAs island on the same site and indium segregation finally creates favorable conditions for a vertically correlated InGaAs non-SK QD system [38] [Fig. 1(b)]. The tuning of the center emission wavelength is performed simply by adjusting the InAs deposition time, yielding to wavelength control and a robust reproducibility.

The active SML QD layers are positioned in the middle between a node and an antinode of the standing electric field intensity wave pattern [Fig. 1(a)]. The QDs are equally spaced with a $\lambda/4$ separation corresponding to 65.5 nm, with the exception of the two most distant active layers from the surface, which present a $\lambda/2$ spacing layer on one side to collect more optically generated carriers and compensate for the exponential decrease of the pump intensity. The average enhancement of the electric field intensity in the SML QDs is set to a low value of 0.5 (normalized to 4 outside the structure) and its spectral profile is designed to be flat over a ± 30-nm bandwidth around the designed center lasing wavelength [Fig. 1(c), inset]. This is not an optimized design for cw performance, where the QD layers will be placed at the antinodes of the standing wave. The epitaxial layer stack is terminated by a 3.5-pair AlAs-Al$_{0.15}$Ga$_{0.85}$As AR section. This VECSEL design is particularly suited for ultrafast operation since it prevents structural spectral filtering of the gain bandwidth and increases the gain saturation fluence with the low field intensity inside the structure.

In contrast to SK QDs but similar to QWs, SML QDs show a non-negligible temperature dependence of the emission and absorption wavelengths [39]. Reflectivity measurements performed on the unpumped SML VECSEL at different temperatures show a thermal redshift of approximately 0.4 nm/K [Fig. 2(a)]. Taking this into account, we set the peak wavelength of the room-temperature photoluminescence (PL) around 1003 nm to obtain a

shifted emission at approximately 1030 nm for an estimated operation temperature of 90 °C. A comparable analysis of the PL intensities emitted under identical experimental conditions by SML QD, QW, and SK QD active test structures with similar interlayer spacing confirms the high modal gain of SML QDs, which deliver the highest intensity [Fig. 2(b)].

The VECSEL is grown in reverse order for standard flip-chip bonding. The DBR, the AR section, and an Al$_{0.85}$Ga$_{0.15}$As etch stop layer are grown at 620 °C, while the GaAs spacers in the active region are grown at 580 °C and the SML QDs at 500 °C. After growth, the chip is indium soldered onto a 5×5 mm^2, 1-mm-thick diamond heat spreader and the GaAs substrate is removed through chemical wet etching. A single fused silica (FS) layer is then deposited with plasma-enhanced chemical vapor deposition (PECVD) to finalize the AR section and obtain a minimized pump reflection at 808 nm together with a flat and low structural group delay dispersion (GDD) for short pulse generation. The difference between designed and measured GDD is explained by growth deviations from the nominal epitaxial layer thickness and deposition errors for the FS layer, estimated to $\pm 1\%$. We obtain a GDD profile in a ± 150 fs^2 range for a 40-nm bandwidth centered at 1030 nm [Fig. 1(c)].

The carrier lifetime in SDLs gives an important indication of the nonradiative losses and represents a crucial parameter for achieving high optical-to-optical pump efficiency in modelocked operation [40,41]. To measure and compare the carrier lifetimes of SML QDs, SK QDs, and QWs, we use a degenerate pump-probe setup with 130-fs pulses and a tunable center pump-probe wavelength, set to the respective PL-maximizing wavelengths of the analyzed gain media. Fitting the saturation recoveries with a double exponential decay, we measure a comparable fast component below 1 ps for the three different structures and

we note sensible differences in the slow components of the recovery time. The QW samples exhibit a slow component of 132 ps [18], significantly shorter than the 406 ps and the 632 ps featured by the SK and SML QDs, respectively. SML QDs seem to offer decreased nonradiative losses and can potentially generate more efficient energetic short pulses.

III. CONTINUOUS WAVE (CW) OPERATION

The SML QD VECSEL chip is tested in a cw straight linear cavity with just the gain mirror and a concave output coupler (OC) used as end mirrors. The chip is mounted on a water-cooled copper heatsink (HS) and pumped with a low-brightness 808-nm diode under a 45° angle. The HS temperature (T_{HS}) is Peltier-controlled and set to −10 °C. No additional intracavity heat spreader is used. The OC features a radius of curvature (ROC) of 200 mm and a transmission of 1%, which delivers the best performance. The total cavity length is set to 75 mm. The focused pump spot is circular on the VECSEL surface with a 177-μm radius; the cavity mode spot size on the chip is calculated to have exactly the same radius. The laser operates in a transverse multimodal regime and the maximum output power of 11.2 W is achieved at an optical pump power of 37 W on the sample. The optical-to-optical efficiency reaches 30% at the maximum power before a thermal roll over occurs. The slope efficiency is 39% [Fig. 3(a)].

We characterize the emission wavelength tunability of the SML QD VECSEL by inserting a 1-mm-thick quartz birefringent filter (BRF) at Brewster's angle inside the optical cavity [Fig. 3(b)]. For this experiment, we obtain the broadest tuning range with a reduced ROC of the output coupler of 100 mm and a smaller laser spot size of 125 μm on the VECSEL. Consequently, the pump spot size is decreased to 135 μm. To compensate for the additional loss introduced by the intracavity filter, we reduce the output coupler to 0.5%. We measure the wavelength-tuning characteristics at a fixed pump power of 18.2 W and a T_{HS} of 0 °C. By rotation of the BRF in its surface plane, we tune the wavelength from 1003 to 1050 nm. The highest output power of 2.43 W is obtained at 1018 nm [Fig. 3(b)]. For a 36-nm span (from 1008 to 1044 nm), the output power exceeds 1 W. The small signal reflectivity of the SML VECSEL is measured on small spot sizes (<20 μm) at a pump intensity of 35 kW/cm^2 and a T_{HS} of 0 °C. The higher total pump power in the tuning experiment increases the temperature of the active region, which is approximately equal to 60 °C, compared to the small signal reflectivity measurements. Considering a thermal wavelength shift of 24 nm, the spectral gain overlaps with the tuning curve in Fig. 3(b).

IV. NOISY MODE-LOCKING OPERATION

The cavity configuration is changed to a standard V shape for the pulsed experiments. The VECSEL chip is used as the folding mirror, while a SESAM and the curved OC serve as end mirrors. The MBE-grown SESAM consists of a single (In_xGa_{1-x})As QW absorber embedded in AlAs barriers on top of a 30-pair GaAs/AlAs DBR. A final $\lambda/4$ Si_3N_4 layer is deposited to increase the field intensity inside the semiconductor. At 1034 nm and 30 °C of heat sink temperature, the measured SESAM saturation fluence is 5.2 μJ/cm^2 and the modulation depth is 1.7%. For the OC, we choose a transmission of 0.5% and a ROC of 100 mm. The pump spot on the chip's surface is set to 177 μm and the laser mode radius is slightly larger (182 μm) to assure single mode operation. For a stronger absorber saturation, the laser spot on the SESAM is focused to a radius of 93 μm. The angle between the two cavity legs is set to 20°; the distances OC-VECSEL and
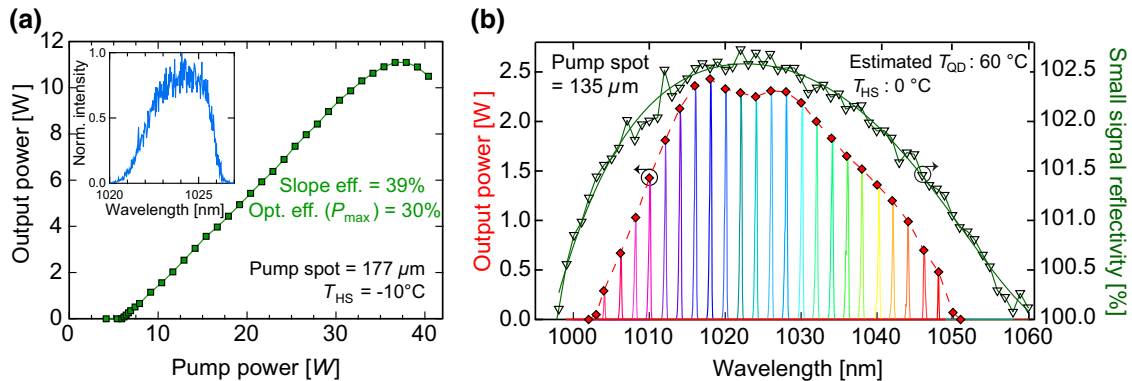

FIG. 3. Cw performance of the SML QD VECSEL. (a) Average output power vs optical pump power characteristic of the SML QD VECSEL at a heatsink temperature of −10 °C. Inset: optical spectrum at 8.5 W of output power. (b) Wavelength tuning characteristic obtained at a constant pump power of 18.2 W, with a wavelength tuning range of 47 nm and 2.43 W of maximum output power at 1018 nm. The measured spectral gain follows the experimental output power profile if a 24-nm redshift is taken into account ($\Delta T \approx 60$ °C). The measured spectra are shown in rainbow colors, scaled to the respective average output power.
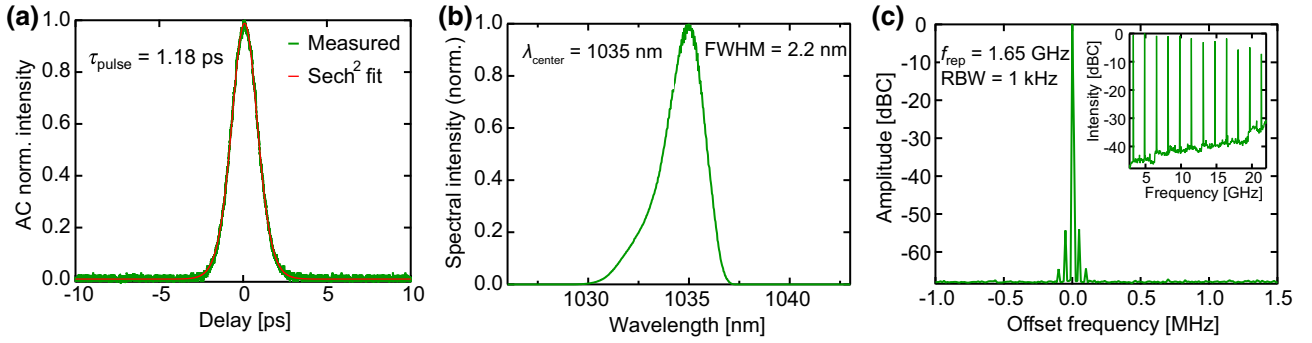
FIG. 4. Ultrafast SML QD VECSEL at low power with unstable modelocking: pulse diagnostics of the SML QD VECSEL pumped with 15.8 W of optical power, just above the lasing threshold of around 15.3 W. We define this mode of operation as unstable modelocking. (a) The noncollinear SHG AC trace can be fitted to a sech^2 pulse shape with a pulse duration of 1.18 ps. (b) The optical spectrum is relatively smooth except for weak noise fringes close to the intensity maximum. (c) The microwave spectrum, recorded with a resolution bandwidth (RBW) of 1 kHz, features a high SNR close to 70 dB in correspondence to the fundamental pulse repetition rate of 1.65 GHz, but we can clearly observe the presence of side peaks. Inset: long span of the microwave spectrum (resolution bandwidth of 300 kHz) showing that all the harmonics of the pulse repetition rate are present with almost equal power.

VECSEL-SESAM are almost balanced and are set to 47 and 44 mm, respectively. A 1-mm-thick wedged intracavity Brewster plate is inserted to obtain a single polarization output.

For a T_{HS} of 0 °C and a SESAM temperature stabilized to 28 °C, we obtain laser light from the VECSEL at 15.3 W of optical pump power. The laser starts in pulsed operation and just above the threshold, for 15.8 W of pump power and 84 mW of average output power, we obtain unstable modelocking which still reveals a rather clean autocorrelation. However, a more careful characterization with a microwave spectrum analyzer clearly reveals the unstable pulsed behavior. The noncollinear second harmonic generation (SHG) autocorrelation (AC) trace is pedestal-free and can be fitted by a sech^2 shape with a pulse duration of 1.18 ps [Fig. 4(a)]. The optical spectrum is centered at 1035 nm and, even if not sech^2-shaped, presents a regular and smooth profile, except for some noisy fringes close to the peak intensity [Fig. 4(b)]. The microwave spectrum features a strong peak corresponding to the fundamental pulse repetition rate of 1.65 GHz, with a high SNR close to 70 dB [Fig. 4(c)]. Small side peaks appear as an indication of nonclean modelocking. The high harmonics of the fundamental pulse repetition rate are all present with almost equal power [Fig. 4(c), inset].

In contrast to what has been reported for ultrafast QW SDLs, where increasing the pump power allowed for the transition from strong pulsations to clean modelocking [42], we observe here that at higher pump levels, we obtain chaotic operation without ever reaching a stable mode-locking situation.

In Fig. 5, we present the diagnostics of the SML QD VECSEL recorded for four different pump powers of 17.2, 18.2, 20.6, and 27.6 W. As the pump power increases, the noncollinear SHG ACs can no longer be fitted to a sech^2

shape. The traces assume a triangular profile with enlarging temporal width and an increasing number of noise spikes. This indicates multiple pulsations rising temporally close to each other. The optical spectra move toward longer wavelengths as a consequence of the increased thermal load. In addition, the spectral profiles become uneven with irregular peaks. Finally, the peaks on the sides of the fundamental repetition rate in the microwave spectrum also grow in intensity; already at 17.2 W of pump power, they appear as nonresolved noise sidebands, suggesting the generation of many pulsations with unstable repetition rates. At 27.6 W of pump power, the intense noise sidebands span over 1 MHz. In the four configurations presented, the average output power rises up to a maximum of 275 mW for a pump power of 27.6 W and an optical-to-optical efficiency of 1%. At higher pump levels, the output power decreases and the laser operation stops without having reached stable modelocking.

V. SIMULATION

Semiconductor gain media show significant refractive index changes after an optical perturbation, usually referred to as amplitude-phase coupling. This effect is commonly quantified through the linewidth enhancement factor α, defined as

$$\alpha = -\frac{4\pi}{\lambda} \frac{dn/dN}{dg/dN}, \tag{1}$$

where n is the refractive index, g is the gain per unit length, λ is the wavelength, and N is the carrier density. Confined structures normally show lower α values due to a clear energetic separation between the active states and their carrier reservoir.
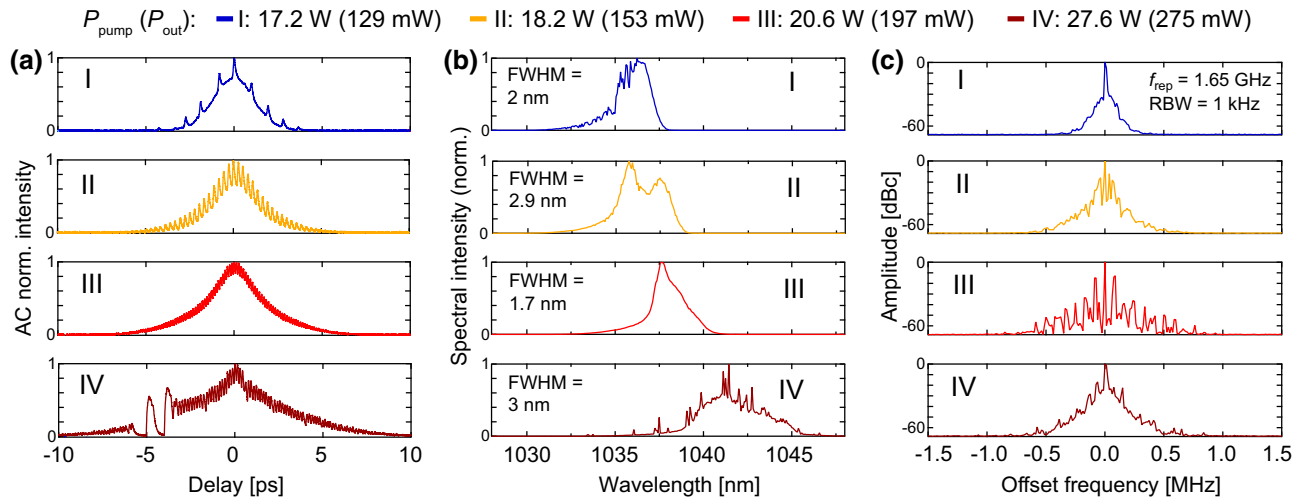
FIG. 5.   Ultrafast SML QD VECSEL with increasing pump power: recorded pulse diagnostics for optical pump powers of I → 17.2 W; II → 18.2 W; III → 20.6 W; IV → 27.6 W. (a) Noncollinear SHG AC traces. As the pump power increases, the traces lose the sech² shape and indicate increasing multiple pulsations. (b) For an increasing pump level, the optical spectra shift toward longer wavelengths and assume irregular spiky shapes. (c) Microwave spectra. At higher pump powers, the side peaks next to the fundamental pulse repetition rate increase their amplitude and can no longer be singularly resolved, finally giving raise to strong and broad noise sidebands.

In SML QDs, the coexistence of 0D and 2D confinement has recently been shown [30]. The heavier holes are better confined in the In-rich islands, while the electron wavefunction sees only the lateral (In_xGa_{1-x})As QW barriers and is delocalized over several InAs agglomerations. This limited confinement in combination with the high areal densities of localization centers enhances a strong interdot coupling in contrast to SK QDs [43]. Furthermore, the efficient lateral coupling with an optically inactive but fast accessible carrier reservoir can provide a very fast gain recovery, but can also induce significant refractive index changes after an optical excitation [44]. Recent measurements revealed linewidth enhancement factors for SML QDs up to one order of magnitude higher compared to SK QDs and QWs [34]. The numerical model for passive modelocking in semiconductor lasers developed by Vladimirov et al. [36] states that if

the linewidth enhancement factor of the gain α_g exceeds the one of the absorber α_a, the modelocking becomes unstable and chaotic. The simulations in [36] show that the most stable operation with the highest-pulse peak powers and shortest-pulse durations can be achieved in the case of $\alpha_g = \alpha_a$. However, in this optimal configuration with a large amplitude-phase coupling, the modelocking breaks up again into a chaotic behavior. Although the parameter space investigated in [36] is not perfectly reproduced with typical VECSEL gain, absorption, and saturation parameters, we have qualitatively observed similar behaviors for the case of $\alpha_g \gg \alpha_a$.

We use our pulse formation model where the pulse is represented by an electric field using the slowly varying envelope approximation (SVEA). We typically start from a 10-nW noise floor and stop when we obtain a numerically stable pulse propagating through the cavity or we

TABLE I.   List of input parameters used for the pulse formation simulation. The input parameters in italics are not directly measured. The SML QD VECSEL saturation fluence is assumed to be comparable to similar QW-based structures [17]. The positive GDD is obtained from the intracavity Brewster's plate. Third order dispersion (TOD) is extraced from the GDD measurement. The gain FWHM used in the simulation is deduced from the output spectra measured in pulsed operation. The SESAM recovery time is defined as the time necessary to reach $1/e$ of the normalized saturation.

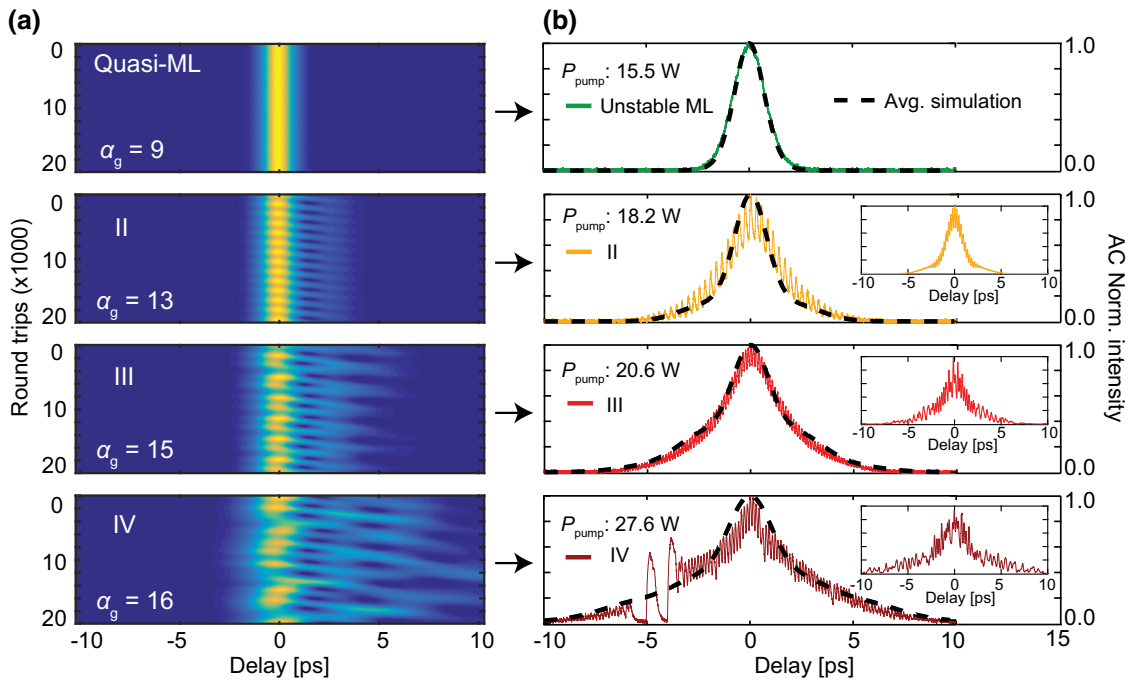| Cavity		Gain		SESAM	
Output coupler	0.5%	Saturation fluence	45 μJ/cm²	Saturation fluence	5 μJ/cm²
Other losses	0.8%	Recovery time	3 ns	Recovery time	1.5–2 ps
Repetition rate	1.65 GHz	α_g	9–17	α_a	2
λ center	1035 nm	Small signal gain	2.9%	Modulation depth	1.8%
GDD	50 fs²	Gain FWHM	5 nm		
TOD	−2000 fs³	Beam radius	170–180 μm	Beam radius	80–100 μm

FIG. 6. Simulation of the mode-locking instabilities with an increasing amplitude-phase coupling in the gain chip. (a) Simulation of the electric field intensity over 20 000 round trips with increasing α_g (color code: yellow → max intensity, blue → zero intensity). (b) Comparison between the measured and the simulated AC traces. The simulated ACs are centered to delay = 0. Dashed black line: simulated AC averaged over 20 000 round trips. Insets: simulated ACs calculated to reproduce the experimental results shown in Figs. 4 and 5. The variable delay line leads to a binning of the time delay axis and to oscillating fringes in the experimental traces in the case of strong intensity fluctuations. The experimental oscillations are qualitatively reproduced by the simulation.

recognize an instability. The different intracavity elements are described by numerical operators either in the time or in the frequency domain and using measurable macroscopic input parameters such as small signal gain, gain bandwidth, GDD profile, and saturation fluences as described in [37,45].

Previous theoretical investigations by Lingnau et al. reported on the failure of the α factor describing dynamical instabilities in SK QD lasers [46]. Later publications by Lingnau et al. concluded, however, that for fast carrier scattering the QD laser behavior can be reasonably well characterized by an α factor [47]. Furthermore, Herzog et al. used the α factor concept to describe the amplitude-phase coupling in SML QDs [34]. For these reasons, we also use the α factor for our description of the carrier induced refractive index changes.

We consider that the amplitude-phase coupling strongly depends on the amount of optically injected carriers [48,49]. Therefore, we set α as a free parameter and increase the strength of the amplitude-phase coupling for higher pump powers. The other simulation parameters for the cavity, VECSEL, and SESAM are listed in Table I; the simulation results are depicted in Fig. 6. Our simulation can confirm the stability breakup of the ML state

by increasing the linewidth enhancement factor in the gain [Fig. 6(a)].

The α values are fitted to obtain a good match of the simulation outputs with the experimental data. For an initial α factor of 9, we still obtain a stable solution with a pulse duration that overlaps with the AC measured for the unstable-ML state [Figs. 4 and 6(b)]. At $\alpha_g = 13$, we observe a transition to a regime of quasi-periodic intensity fluctuations. The averaged AC computed from the simulation matches with state II experimentally measured in the SML VECSEL cavity (Fig. 5).

A more pronounced effect is produced with $\alpha_g = 15$: a chaotic pattern of intensity oscillations occurs, with intermittent buildup and breakup phases of the main pulse. This regime gives an output, which is comparable in terms of the AC observed in the SML VECSEL for 20.6 W of pump power (state III in Fig. 5).

Finally, we set $\alpha_g = 16$, which results in a fully chaotic regime with unstable spikings. The simulated averaged AC output is similar to that observed for 27.6 W of pump power in state IV in Fig. 5.

The estimated α values between 9 and 16 are significantly higher compared to the α range assumed for SK QDs and QWs (normally between 2 and 10 [50–52]). They

are consistent with the directly measured values reported in [34] for optical semiconductor amplifiers based on SML QDs.

VI. CONCLUSIONS

In this work, we test the potential of SML QDs as active gain media for ultrafast SDLs. In particular, we want to take advantage of the high modal gain of SML QDs for efficient generation of energetic ultrashort pulses. Therefore, we grow a VECSEL chip with 10 SML QD gain layers. This VECSEL structure is designed and optimized to produce fs pulses at 1030 nm. Tests performed in cw confirm the excellent gain properties of QD grown following the SML technique compared to other epitaxial methods for QD formation. We obtain the highest average output power of 11.2 W ever generated from QD-based SDLs. To confirm the large gain bandwidth necessary for short pulse duration, we use the VECSEL as a high-power tunable cw source, obtaining a lasing operation over 47 nm.

In a second experiment, we insert a SESAM in the optical cavity to passively modelock the SML QD VECSEL. In this configuration, we do not obtain a regime of stable fundamental modelocking. We observe strong instabilities that prevent the formation of short femtosecond pulses and show clear symptoms of chaotic multiple pulsations already appearing at pump levels slightly above the lasing threshold. We take into account the recent research on the strong amplitude-phase coupling shown by SML QDs and simulate the output of the unstable ultrafast SML QD VECSEL with a pulse formation model based on measurable macroscopic input parameters such as small signal gain, gain bandwidth, GDD profile, and saturation fluences. We observe that the intrinsically large α value for SML QDs can prevent the formation of stable modelocked solutions in the laser cavity, as predicted by other theories [36]. In addition, by fitting the simulated results with the experimental traces and adjusting only the linewidth enhancement factor, we can argue that the mode-locking instabilities can be related to an increase of the linewidth enhancement factor at higher injections of optically generated carriers. With our results, we confirm the great benefits of optically pumped SML QD VECSELs for high-power cw outputs and large wavelength tuning. On the other side, we recognize that due to intrinsic physical properties connected to the growth method, SML QDs are not suitable for stable modelocking.

ACKNOWLEDGMENTS

[1] M. Guina, A. Rantamäki, and A. Härkönen, Optically pumped VECSELs: Review of technology and progress, J. Phys. D: Appl. Phys. **50**, 383001 (2017).

[2] B. W. Tilma, M. Mangold, C. A. Zaugg, S. M. Link, D. Waldburger, A. Klenner, A. S. Mayer, E. Gini, M. Golling, and U. Keller, Recent advances in ultrafast semiconductor disk lasers, Light Sci. Appl. **4**, e310 (2015).

[3] U. Keller and A. C. Tropper, Passively modelocked surface-emitting semiconductor lasers, Phys. Rep. **429**, 67 (2006).

[4] D. J. H. C. Maas, A.-R. Bellancourt, B. Rudin, M. Golling, H. J. Unold, T. Südmeyer, and U. Keller, Vertical integration of ultrafast semiconductor lasers, Appl. Phys. B **88**, 493 (2007).

[5] S. M. Link, D. J. H. C. Maas, D. Waldburger, and U. Keller, Dual-comb spectroscopy of water vapor with a free-running semiconductor disk laser, Science **356**, 1164 (2017).

[6] F. F. Voigt, F. Emaury, P. Bethge, D. Waldburger, S. M. Link, S. Carta, A. v. d. Bourg, F. Helmchen, and U. Keller, Multiphoton in vivo imaging with a femtosecond semiconductor disk laser, Biomed. Opt. Express **8**, 3213 (2017).

[7] B. Heinen, T. L. Wang, M. Sparenberg, A. Weber, B. Kunert, J. Hader, S. W. Koch, J. V. Moloney, M. Koch, and W. Stolz, 106 W continuous-wave output power from vertical-external-cavity surface-emitting laser, Electron. Lett. **48**, 516 (2012).

[8] U. Keller, K. J. Weingarten, F. X. Kärtner, D. Kopf, B. Braun, I. D. Jung, R. Fluck, C. Hönninger, N. Matuschek, and J. Aus der Au, Semiconductor saturable absorber mirrors (SESAMs) for femtosecond to nanosecond pulse generation in solid-state lasers, IEEE J. Sel. Top. Quantum. Electron. **2**, 435 (1996).

[9] S. Hoogland, S. Dhanjal, A. C. Tropper, S. J. Roberts, R. Häring, R. Paschotta, and U. Keller, Passively mode-locked diode-pumped surface-emitting semiconductor laser, IEEE Photon. Technol. Lett. **12**, 1135 (2000).

[10] B. Rudin, V. J. Wittwer, D. J. H. C. Maas, M. Hoffmann, O. D. Sieber, Y. Barbarin, M. Golling, T. Südmeyer, and U. Keller, High-power MIXSEL: An integrated ultrafast semiconductor laser with 6.4 W average power, Opt. Express **18**, 27582 (2010).

[11] M. Hoffmann, O. D. Sieber, V. J. Wittwer, I. L. Krestnikov, D. A. Livshits, Y. Barbarin, T. Südmeyer, and U. Keller, Femtosecond high-power quantum dot vertical external cavity surface emitting laser, Opt. Express **19**, 8108 (2011).

[12] M. Mangold, C. A. Zaugg, S. M. Link, M. Golling, B. W. Tilma, and U. Keller, Pulse repetition rate scaling from 5 GHz to 100 GHz with a high-power semiconductor disk laser, Opt. Express **22**, 6099 (2014).

[13] M. Mangold, S. M. Link, A. Klenner, C. A. Zaugg, M. Golling, B. W. Tilma, and U. Keller, Amplitude noise

and timing jitter characterization of a high-power mode-locked integrated external-cavity surface emitting laser, IEEE Photon. J. **6,** 1 (2014).

[14] S. M. Link, A. Klenner, M. Mangold, C. A. Zaugg, M. Golling, B. W. Tilma, and U. Keller, Dual-comb mode-locked laser, Opt. Express **23,** 5521 (2015).

[15] N. Jornod, K. Gürel, V. J. Wittwer, P. Brochard, S. Hakobyan, S. Schilt, D. Waldburger, U. Keller, and T. Südmeyer, Carrier-envelope offset frequency stabilization of a gigahertz semiconductor disk laser, Optica **4,** 1482 (2017).

[16] C. A. Zaugg, A. Klenner, M. Mangold, A. S. Mayer, S. M. Link, F. Emaury, M. Golling, E. Gini, C. J. Saraceno, B. W. Tilma, and U. Keller, Gigahertz self-referencable frequency comb from a semiconductor disk laser, Opt. Express **22,** 16445 (2014).

[17] D. Waldburger, S. M. Link, M. Mangold, C. G. E. Alfieri, E. Gini, M. Golling, B. W. Tilma, and U. keller, High-power 100 fs semiconductor disk lasers, Optica **3,** 844 (2016).

[18] C. G. E. Alfieri, D. Waldburger, S. M. Link, E. Gini, M. Golling, G. Eisenstein, and U. Keller, Optical efficiency and gain dynamics of modelocked semiconductor disk lasers, Opt. Express **25,** 6402 (2017).

[19] I. Kilen, J. Hader, J. V. Moloney, and S. W. Koch, Ultrafast nonequilibrium carrier dynamics in semiconductor laser mode locking, Optica **1,** 192 (2014).

[20] D. Bimberg, N. Kirstaedter, and N. N. Ledentsov, InGaAs-GaAs quantum-dot lasers, IEEE J. Sel. Top. Quantum. Electron. **3,** 196 (1997).

[21] T. W. Berg and J. Mork, Saturation and noise properties of quantum-dot optical amplifiers, IEEE J. Quantum. Electron. **40,** 1527 (2004).

[22] J. Gomis-Bresco, S. Dommers, V. V. Temnov, U. Woggon, M. Laemmlin, D. Bimberg, E. Malic, M. Richter, E. Schöll, and A. Knorr, Impact of Coulomb Scattering on the Ultrafast Gain Recovery in InGaAs Quantum Dots, Phys. Rev. Lett. **101,** 256803 (2008).

[23] M. Butkus, J. Rautiainen, O. G. Okhotnikov, C. J. Hamilton, G. P. A. Malcolm, S. S. Mikhrin, I. L. Krestnikov, D. A. Livshits, and E. U. Rafailov, Quantum dot based semiconductor disk lasers for 1–1.3 μm, IEEE J. Sel. Top. Quantum. Electron. **17,** 176 (2011).

[24] C. G. E. Alfieri, D. Waldburger, M. Golling, and U. Keller, High-power sub-300-femtosecond quantum dot semiconductor disk lasers, IEEE Photonics Technol. Lett. **30,** 525 (2018).

[25] N. A. Cherkashin, M. V. Maksimov, A. G. Makarov, V. A. Shchukin, V. M. Ustinov, N. V. Lukovskaya, Y. G. Musikhin, G. E. Cirlin, N. A. Bert, Z. I. Alferov, N. N. Ledentsov, and D. Bimberg, Control over the parameters of InAs-GaAs quantum dot arrays in the Stranski-Krastanow growth mode, Semiconductors **37,** 861 (2003).

[26] S. Gaan, G. He, R. M. Feenstra, J. Walker, and E. Towe, Size, shape, composition, and electronic properties of InAs/GaAs quantum dots by scanning tunneling microscopy and spectroscopy, J. Appl. Phys. **108,** 114315 (2010).

[27] D. A. Nakdali, M. K. Shakfa, M. Gaafar, M. Butkus, K. A. Fedorova, M. Zulonas, M. Wichmann, F. Zhang, B. Heinen, A. Rahimi-Iman, W. Stolz, E. U. Rafailov, and M. Koch,

High-power quantum-dot vertical-external-cavity surface-emitting laser exceeding 8 W, IEEE Photonics Technol. Lett. **26,** 1561 (2014).

[28] S. Krishna, D. Zhu, J. Xu, K. K. Linder, O. Qasaimeh, P. Bhattacharya, and D. L. Huffaker, Structural and luminescence characteristics of cycled submonolayer InAs/GaAs quantum dots with room-temperature emission at 1.3 μm, J. Appl. Phys. **86,** 6135 (1999).

[29] A. Lenz, H. Eisele, J. Becker, J.-H. Schulze, T. D. Germann, F. Luckert, K. Pötschke, E. Lenz, L. Ivanova, A. Strittmatter, D. Bimberg, U. W. Pohl, and M. Dähne, Atomic structure and optical properties of InAs submonolayer depositions in GaAs, J. Vac. Sci. Technol. B: Microelectron. Nanometer. Struct. Process. Meas. Phenom. **29,** 04D104 (2011).

[30] S. Harrison, M. P. Young, P. D. Hodgson, R. J. Young, M. Hayne, L. Danos, A. Schliwa, A. Strittmatter, A. Lenz, H. Eisele, U. W. Pohl, and D. Bimberg, Heterodimensional charge-carrier confinement in stacked submonolayer InAs in GaAs, Phys. Rev. B **93,** 085302 (2016).

[31] F. Hopfer, A. Mutig, G. Fiol, M. Kuntz, V. A. Shchukin, V. A. Haisler, T. Warming, E. Stock, S. S. Mikhrin, I. L. Krestnikov, D. A. Livshits, A. R. Kovsh, C. Bornholdt, A. Lenz, H. Eisele, M. Dahne, N. N. Ledentsov, and D. Bimberg, 20 Gb/s 85°C error-free operation of VCSELs based on submonolayer deposition of quantum dots, IEEE J. Sel. Top. Quantum. Electron. **13,** 1302 (2007).

[32] N. N. Ledentsov, D. Bimberg, F. Hopfer, A. Mutig, V. A. Shchukin, A. V. Savel'ev, G. Fiol, E. Stock, H. Eisele, M. Dähne, D. Gerthsen, U. Fischer, D. Litvinov, A. Rosenauer, S. S. Mikhrin, A. R. Kovsh, N. D. Zakharov, and P. Werner, Submonolayer quantum dots for high speed surface emitting lasers, Nanoscale Res. Lett. **2,** 417 (2007).

[33] T. D. Germann, A. Strittmatter, J. Pohl, U. W. Pohl, D. Bimberg, J. Rautiainen, M. Guina, and O. G. Okhotnikov, High-power semiconductor disk laser based on InAs/GaAs submonolayer quantum dots, Appl. Phys. Lett. **92,** 101123 (2008).

[34] B. Herzog, B. Lingnau, M. Kolarczik, Y. Kaptan, D. Bimberg, A. Maaßdorf, U. W. Pohl, R. Rosales, J.-H. Schulze, A. Strittmatter, M. Weyers, U. Woggon, K. Lüdge, and N. Owschimikow, Strong amplitude-phase coupling in submonolayer quantum dots, Appl. Phys. Lett. **109,** 201102 (2016).

[35] B. Lingnau, K. Lüdge, B. Herzog, M. Kolarczik, Y. Kaptan, U. Woggon, and N. Owschimikow, Ultrafast gain recovery and large nonlinear optical response in submonolayer quantum dots, Phys. Rev. B **94,** 014305 (2016).

[36] A. G. Vladimirov and D. Turaev, Model for passive mode locking in semiconductor lasers, Phys. Rev. A **72,** 033808 (2005).

[37] O. D. Sieber, M. Hoffmann, V. J. Wittwer, M. Mangold, M. Golling, B. W. Tilma, T. Südmeyer, and U. Keller, Experimentally verified pulse formation model for high-power femtosecond VECSELs, Appl. Phys. B **113,** 133 (2013).

[38] V. A. Shchukin, D. Bimberg, V. G. Malyshkin, and N. N. Ledentsov, Vertical correlations and anticorrelations in multisheet arrays of two-dimensional islands, Phys. Rev. B **57,** 12262 (1998).

[39] D. Arsenijevic, C. Liu, A. Payusov, M. Stubenrauch, and D. Bimberg, Temperature-dependent characteristics of single-mode InAs submonolayer quantum-dot lasers, IEEE Photonics Technol. Lett. **24,** 906 (2012).

[40] A. Laurain, J. Hader, Y.-Y. Lai, T.-L. Wang, M. Yarborough, G. Balakrishnan, T. J. Rotter, P. Ahirwar, and J. V. Moloney, Influence of non-radiative carrier losses on pulsed and continuous VECSEL performance, in *SPIE LASE* (SPIE, San Francisco, 2012), 8242.

[41] M. M. Karow, N. N. Faleev, A. Maros, and C. B. Honsberg, Defect creation in InGaAs/GaAs multiple quantum wells − II. Optical properties, J. Cryst. Growth **425,** 49 (2015).

[42] M. Mangold, M. Golling, E. Gini, B. W. Tilma, and U. Keller, Sub-300-femtosecond operation from a MIXSEL, Opt. Express **23,** 22043 (2015).

[43] B. Lingnau, B. Herzog, M. Kolarczik, U. Woggon, K. Lüdge, and N. Owschimikow, Dynamic phase response and amplitude-phase coupling of self-assembled semiconductor quantum dots, Appl. Phys. Lett. **110,** 241102 (2017).

[44] B. Herzog, N. Owschimikow, J.-H. Schulze, R. Rosales, Y. Kaptan, M. Kolarczik, T. Switaiski, A. Strittmatter, D. Bimberg, U. W. Pohl, and U. Woggon, Fast gain and phase recovery of semiconductor optical amplifiers based on submonolayer quantum dots, Appl. Phys. Lett. **107,** 201102 (2015).

[45] R. Paschotta, R. Häring, U. Keller, A. Garnache, S. Hoogland, and A. C. Tropper, Soliton-like pulse-shaping mechanism in passively mode-locked surface-emitting semiconductor lasers, Appl. Phys. B **75,** 445 (2002).

[46] B. Lingnau, K. Lüdge, W. W. Chow, and E. Schöll, Failure of the α factor in describing dynamical instabilities and chaos in quantum-dot lasers, Phys. Rev. E **86,** 065201 (2012).

[47] B. Lingnau, W. W. Chow, and K. Lüdge, Amplitude-phase coupling and chirp in quantum-dot lasers: Influence of charge carrier scattering dynamics, Opt. Express **22,** 4867 (2014).

[48] F. Grillot, B. Dagens, J. G. Provost, H. Su, and L. F. Lester, Gain compression and above-threshold linewidth enhancement factor in 1.3 µm InAs-GaAs quantum-dot lasers, IEEE J. Quantum. Electron. **44,** 946 (2008).

[49] S. Melnik, G. Huyet, and A. V. Uskov, The linewidth enhancement factor α of quantum dot semiconductor lasers, Opt. Express **14,** 2950 (2006).

[50] T. C. Newell, D. J. Bossert, A. Stintz, B. Fuchs, K. J. Malloy, and L. F. Lester, Gain and linewidth enhancement factor in InAs quantum-dot laser diodes, IEEE Photonics Technol. Lett. **11,** 1527 (1999).

[51] T. Ohtoshi and N. Chinone, Linewidth enhancement factor in strained quantum well lasers, IEEE Photonics Technol. Lett. **1,** 117 (1989).

[52] A. A. Ukhanov, A. Stintz, P. G. Eliseev, and K. J. Malloy, Comparison of the carrier induced refractive index, gain, and linewidth enhancement factor in quantum dot and quantum well lasers, Appl. Phys. Lett **84,** 1058 (2004).